Cooperative manipulation of deformable objects by single-leader-dual-follower teleoperation

Article (Accepted Version)

Cooperative Manipulation of Deformable Objects by Single-Leader-Dual-Follower Teleoperation

Darong Huang, Bin Li, Yanan Li, *Senior Member*, and Chenguang Yang, *Senior Member*

***Abstract*—This paper proposes a method for single-leader-dual-follower (SLDF) teleoperation, where one robot (direct-follower robot, DFR) is directly teleoperated and the other robot (assisting-follower robot, AFR) can autonomously cooperate with DFR to hold and move a deformable object, with the contact force regulated to a desired value. Since AFR does not know its partner's movement, firstly, it achieves position alignment with DFR by using the contact force. Secondly, we develop an adaptive movement estimation algorithm according to Lyapunov theory, such that DFR's position is estimated in the presence of dynamic uncertainties. Finally, we adopt the impedance control to generate a reference trajectory for AFR to track, in order to maintain the desired contact force. Several simulations are conducted on a platform with two three-degrees-of-freedom (3-DOFs) robots. Experiments are performed with a dual-arm robot (Baxter), results of which demonstrate the feasibility and effectiveness of the proposed method.**

***Index Terms*—Contact force regulation, impedance controller, movement estimation, multi-robot collaboration, single-leader-dual-follower teleoperation**

I. Introduction

ROBOT teleoperation is widely implemented in applications of manufacturing [1], healthcare [2], search and rescue [3], aerospace [4] [5] and marine exploration [6]–[8], military [6] etc., which enables human operators to stay in a comfortable and safe place to control robots working on hazardous experiments. Within this field, alleviating human's cognitive and physical burdens is an emerging topic in recent years. Comparing to multiple-leader-multiple-follower (MLMF) teleoperation [9], employing one leader robot to teleoperate multiple tele-robots [10] [11] reduces operators' cognitive burden. Comparing to single-leader-single-follower (SLSF) [12] [13] or multiple-leader-single-follower (MLSF) [14] robot teleoperation, it has the ability to handle more complicated tasks thanks to tele-robots' collaboration.

Manuscript received Month xx, 2xxx; revised Month xx, xxxx; accepted Month x, xxxx. This work was supported in part by National Nature Science Foundation of China (NSFC) under Grant U20A20200 and 61861136009, in part by Guangdong Basic and Applied Basic Research Foundation under Grants 2019B1515120076 and 2020B1515120054, in part by Industrial Key Technologies R & D Program of Foshan under Grant 2020001006496 and Grant 2020001006308. *(Corresponding author: Chenguang Yang.)*

D. Huang, B. Li and C. Yang are with School of Automation Science and Engineering, South China University of Technology, Guangzhou, 510641, China (email: bamboo_hdr@163.com; bingo_lb@163.com; cyang@ieee.org).

Y. Li is with School of Engineering and Informatics, University of Sussex, Brighton, BN1 9QJ, UK (email: yl557@sussex.ac.uk).

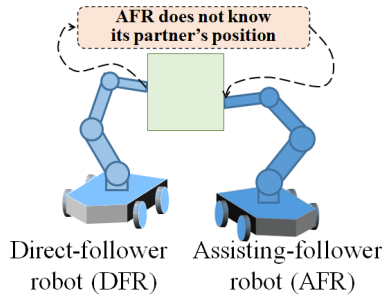

Fig. 1. An AFR needs to manipulate an object in collaboration with a DFR whose movement is controlled by a human operator and unknown to AFR.

Due to these unique advantages, single-leader-multiple-follower (SLMF) robot teleoperation is widely investigated. While many SLMF works are about multiple mobile robots [15] [10], manipulators are the main focus of this paper, where their cooperation is achieved via physical contact. [11] investigated the regulation of dual tele-robots' position, orientation and force in single-leader-dual-follower (SLDF) teleoperation. [16] developed a vision-based framework, enabling one tele-robot to semi-autonomously assist a tele-robot to perform minimally invasive surgery. [17] developed an approach for some ubiquitous surgical tasks, e.g., suturing, by using SLDF teleoperation.

The aforementioned SLMF teleoperation literature has an assumption that the follower robots can share information, e.g., their poses, with each other. However, there are many cases where AFR needs to cooperate with DFR, but they do not have direct communication. As shown in Fig. 1, while DFR is directly tele-operated by a human, AFR needs to modulate its own movement for successful manipulation of the object. Since these two follower robots are in physical interaction through a common object, DFR's movement may be estimated by AFR using the information of interaction force. Moreover, as for manipulation of deformable objects such as organs, tissues, cables and household laundries [18]–[20], researchers presented practical methods to endow the manipulator with touching sense [21] and achieve high-precision force tracking when interacting with soft objects [22] [23]. These works shared the same idea that a robot can use the contact force to modulate its movement. They also revealed challenges in addressing the problems when the objects' information is entirely unknown.

To address all the concerns mentioned-above, the proposed method in this paper has its unique properties for followers'

collaboration in manipulating a deformable object, listed as below:

- Comparing to previous works [11], [16], [17] where both tele-robots exchange pose information with each other, in this paper, two tele-robots do not know their partner's pose and their collaboration is achieved based on merely the contact force. Different from traditional passive impedance control [24]–[27], we enable AFR to estimate its partner's movement, leading to an explicit contact force control.
- Comparing to [28] and its extensions like [29]–[31], instead of dealing with an environment with a fixed rest position, the proposed method enables AFR to interact with an environment with a time-varying rest position (because the contact surface moves as DFR moves), without requiring the knowledge of the environmental movements and interaction model parameters.

The rest of this paper is organized as follows: Section II describes potential problems in the SLDF teleoperation when the two tele-robots do not exchange information; Section III develops an adaptation scheme for AFR, including regulation of the holding pose, estimation of the unknown lumped movement of DFR and the held object, and derivation of the reference trajectory for AFR; Section IV illustrates the simulations conducted on a platform with two 3-DOFs robots and experiments on a Baxter robot; Section V concludes the paper.

II. Problem Formulation

A. System Description

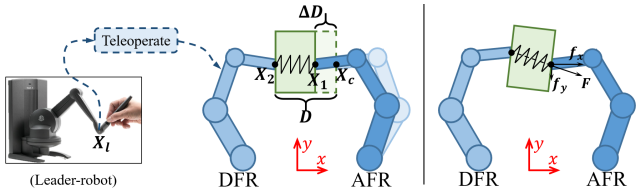

Fig. 2. Single-leader-dual-follower teleoperation system. DFR is under the leader robot's control and its movement is unknown to AFR.

The system setup to be discussed in this paper is shown in Fig. 2, where the leader robot is manipulated by an operator, and its position $X_l = [x_l, y_l, z_l]^T$ is conveyed to DFR, and AFR assists DFR in holding and moving a deformable object.

As X_l is directly from the leader, the desired position for DFR is

$$X_{2,d} = sRX_l, \tag{1}$$

where $X_{2,d} = [x_{2,d}, y_{2,d}, z_{2,d}]^T$, R is the rotation matrix which transforms the leader robot's coordinate to the tele-robots' coordinate and s is a scaling factor to be selected according to different implementation scenarios.

Since we focus on the controller design for AFR, its dynamics equation is given as

$$M_1(q)\ddot{q} + C_1(q,\dot{q})\dot{q} + G_1(q) = \tau + J_1(q)^T F, \tag{2}$$

where q, $\dot{q}$ and $\ddot{q}$ are respectively the joint position, velocity, and acceleration of AFR; $M_1(q)$, $C_1(q,\dot{q})$, $G_1(q)$ and $J_1(q)$ represent the inertial matrix, Coriolis and centrifugal matrix, gravity vector and Jacobian matrix of AFR, respectively; τ denotes the control torque for each joint; $F = [f_x, f_y, f_z]^T$ stands for the force between AFR and the object and f_x, f_y and f_z are components of F in x, y z directions. Within the discussion of this paper, the point contact between the robots and the object is considered, i.e., F in Eq. (3) *contains no torques*.

Assumption 1: The object held by two robots is assumed to be a spring connecting two EEs and its mass is supposed to be small enough to be neglectable, or is considered estimable [32] such that its affect can be compensated for. Thus, the following development leaves out the object's mass for brevity.

Based on Assumption 1, in accordance with the dynamics of a spring, we have

$$||F|| = k_o||\Delta D||, \tag{3}$$

where $||F||$ is the holding force of the spring; $\Delta D = [\Delta D_x, \Delta D_y, \Delta D_z]^T$ with ΔD_x, ΔD_y and ΔD_z standing for the increment components between two EEs' displacement in the x, y and z directions; $||\Delta D||$ represents the deformation of the virtual spring; k_o denotes the Hooke's coefficient of the spring; and "$||\cdot||$" stands for 2-norm operator. Then, it is easy to obtain

$$F = k_o \Delta D. \tag{4}$$

As shown in Fig. 2, the increment is

$$\Delta D = D - (X_1 - X_2), \tag{5}$$

where $X_1 = [x_1, y_1, z_1]^T$ and $X_2 = [x_2, y_2, z_2]^T$ represent AFR and DFR's positions respectively and $D = [D_x, D_y, D_z]^T$ stands for the distance between two EEs when the spring is at its rest position, i.e. not deformed. X_1 and X_2 in Eq. (5) are coordinates in AFR's frame and X_2 is an unknown and time-varying variable. Now, we take the object and DFR as a whole, which is a dynamical environment from AFR's perspective. We define this environment's rest position as X_c (when the object is not deformed), then the contact force becomes

$$F = k_o(X_c - X_1), \tag{6}$$

where

$$X_c = [x_c, y_c, z_c]^T = D + X_2, \tag{7}$$

which is time-varying because of DFR's unknown movement.

Remark 1: It should be pointed out that ΔD should satisfy a condition $0 < \Delta D_{min} < \Delta D < \Delta D_{max}$, where ΔD_{min} is a minimum value to trigger the excitation for parameters estimation and ΔD_{max} is set for system safety purpose. This condition will certainly become the constraint to X_c: $\Delta D_{min} + X_1 < X_c < \Delta D_{max} + X_1$. It means that X_c must deviate from X_1 but can not move too far away from X_1 at every instant. In this paper, we technically set bounds for X_c to acquire signal excitations and achieve system safety.

B. Problem Statement

The key objective for the SLDF teleoperation presented in Section II-A is to control AFR to collaborate with its partner, DFR, which is directly under the leader's (operator's) control. As X_2 is time-varying and unknown to AFR, AFR's trajectory should be carefully designed, which is the main problem to be addressed in this paper.

The task for AFR and DFR is to cooperatively hold and move a deformable object, where the only information known to AFR is the contact force F. To this end, based on F, we firstly need to regulate AFR's position to maintain holding according to DFR's movement; and secondly, a proper trajectory needs to be generated for AFR such that the object's holding force (the contact force F) converges to a desired value.

To simplify the problems, we point out that the situation we consider in this paper is that two robots hold a deformable object in a hinge-like manner, where no torque is generated between the object and the two robots, unlike grasping, gripping or clamping an object [33]–[35]. Therefore, we do not consider rotations but only translations of the object.

III. Adaptation Scheme

Corresponding to problems stated in Section II-B, the proposed method can be divided into three steps: maintaining the holding position of AFR when the object is being translated; estimating X_c that lumps DFR's movement and the object's deformation; and generating a reference trajectory based on impedance control for AFR such that the object's holding force is maintained around the desired value.

A. Holding Regulation

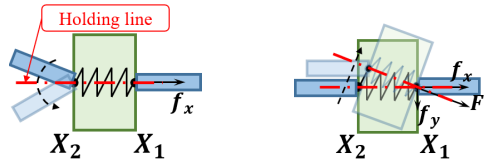

(a) No changes on F as DFR rotates. (b) F changes as DFR moves.

Fig. 3. Contact force on AFR changes depending on DFR's movement.

As there is no torque in F, the object is not expected to rotate in this paper, shown in Fig. 3(a). When DFR translates, AFR should translate in accordance, e.g. AFR should move upwards in Fig. 3(b) as DFR moves upwards. For this purpose, the *holding line* is defined when the contact force is in the horizontal direction, i.e. along x-axis direction in the case of Fig. 3. Therefore, the other components of F (f_y and f_z) should be controlled to zero by adjusting y and z positions via

$$\Delta y_1 = -k_y f_y, \tag{8}$$

$$\Delta z_1 = -k_z f_z, \tag{9}$$

where Δy_1 and Δz_1 denote desired displacements for AFR in the y and z-directions, $k_y > 0$, $k_z > 0$ and they stand for the user defined adaptation gains.

The adaptation scheme in Eqs. (8) and (9) makes AFR move against the directions of f_y and f_z until Δy_1 and $\Delta z_1 \to 0$ when f_y and $f_z \to 0$, e.g., AFR should move upwards as f_y points downwards in Fig. 3(b), which is under a condition that the object has already been compressed. Consequently, AFR will not move away from the holding line and thus the holding line can be maintained along the x axis. Roughly speaking, the adaptation scheme in Eq. (8) and (9) can be interpreted as a special case of feedback force controllers $\Delta y_1 = -k_y(f_y - f_{y,d})$ and $\Delta z_1 = -k_z(f_z - f_{z,d})$, where desired forces $f_{y,d} = 0$ and $f_{z,d} = 0$.

Remark 2: Since we have handled issues regarding y_1 and z_1, i.e., AFR's movement is regulated to stay on the holding line. In the following development, we focus on the regulation of x_1, related to x_c and f_x, which are one dimensional variables.

B. Unknown Movement Estimation

In this subsection, we will use the force f_x to estimate the unknown time-varying position x_c, which is critical for generating $x_{1,d}$ in Section III-C. Generally, we can model x_c to be a time-varying trajectory as

$$x_c(t) = a_0 + a_1 t + a_2 t^2 + \cdots + a_{n-1} t^{n-1}. \tag{10}$$

where t represents time and a_{n-1} with $n = 1, 2, 3, \cdots$ are considered to be constants during a certain period of time. Thus, the corresponding velocity and acceleration are

$$\begin{aligned} \dot{x}_c(t) &= a_1 + 2a_2 t + \cdots + (n-1)a_{n-1} t^{n-2}, \\ \ddot{x}_c(t) &= 2a_2 + \cdots + (n-1)(n-2)a_{n-1} t^{n-3}. \end{aligned} \tag{11}$$

where, without loss of generality, we take $n = 3$ in the rest of discussion for simplicity of analysis.

Based on the model in Eq. (10), the estimate of x_c is described as

$$\begin{aligned} \hat{x}_c &= \hat{a}_0 + \hat{a}_1 t + \hat{a}_2 t^2, \\ \dot{\hat{x}}_c &= \hat{a}_1 + 2\hat{a}_2 t, \\ \ddot{\hat{x}}_c &= 2\hat{a}_2, \end{aligned} \tag{12}$$

where $\hat{*}$ is the estimate of $*$. Then, we define

$$\hat{f}_x = \hat{k}_o(\hat{x}_c - x_1), \tag{13}$$

where $\hat{f}_x$ and $\hat{k}_o$ are the estimated force and the object's Hooke's coefficient, respectively. Subtracting Eq. (6) by Eq. (13), we obtain

$$\begin{aligned} \hat{f}_x - f_x &= \hat{k}_o(\hat{a}_0 + \hat{a}_1 t + \hat{a}_2 t^2 - x_1) \\ &\quad - k_o(a_0 + a_1 t + a_2 t^2 - x_1) \\ &= [x_1 \quad 1 \quad t \quad t^2]\Phi, \end{aligned} \tag{14}$$

where

$$\Phi = \begin{bmatrix} -\hat{k}_o + k_o \\ \hat{k}_o\hat{a}_0 - k_o a_0 \\ \hat{k}_o\hat{a}_1 - k_o a_1 \\ \hat{k}_o\hat{a}_2 - k_o a_2 \end{bmatrix}, \tag{15}$$

which denotes the estimation errors of the unknown lumped dynamical parameters.

According to Lyapunov theory, we design an adaptive updating law for Φ,

$$\dot{\Phi} = \begin{bmatrix} -\dot{\hat{k}}_o \\ \dot{\hat{k}}_o\hat{a}_0 + \hat{k}_o\dot{\hat{a}}_0 \\ \dot{\hat{k}}_o\hat{a}_1 + \hat{k}_o\dot{\hat{a}}_1 \\ \dot{\hat{k}}_o\hat{a}_2 + \hat{k}_o\dot{\hat{a}}_2 \end{bmatrix} = -\Gamma^{-1} \begin{bmatrix} x_1 \\ 1 \\ t \\ t^2 \end{bmatrix} (\hat{f}_x - f_x), \tag{16}$$

i.e., adaptive updating laws for $\hat{k}_o$ and $\hat{a}_i$,

$$\dot{\hat{k}}_o = \gamma_1^{-1} x_1 (\hat{f}_x - f_x), \tag{17}$$

$$\dot{\hat{a}}_{j-1} = -\frac{1}{\hat{k}_o}(\gamma_{j+1}^{-1} t^{j-1}(\hat{f}_x - f_x) + \dot{\hat{k}}_o \hat{a}_{j-1}), j = 1, 2, 3 \tag{18}$$

where the updating rate γ_j in Eqs. (17) and (18) belongs to the positive definite matrix $\Gamma = \text{diag}[\gamma_1, \gamma_2, \gamma_3, \gamma_4]$ in Eq. (16). In the following equations, we show that the adaptation laws in Eqs. (15)-(17) make the force estimation error $\hat{f}_x - f_x$ converge to 0.

Let us construct a Lyapunov function as

$$V = \frac{1}{2}\Phi^T \Gamma \Phi. \tag{19}$$

Differentiating Eq. (19), with respect to time, yields

$$\dot{V} = \Phi^T \Gamma \dot{\Phi}. \tag{20}$$

Taking the transpose of both sides of Eq. (14), we have

$$(\hat{f}_x - f_x)^T = \Phi^T \begin{bmatrix} x_1 \\ 1 \\ t \\ t^2 \end{bmatrix}. \tag{21}$$

Substituting the adaptive updating law (16) into Eq. (20), and considering Eq. (21), we have

$$\dot{V} = -\Phi^T \begin{bmatrix} x_1 \\ 1 \\ t \\ t^2 \end{bmatrix} (\hat{f}_x - f_x) = -(\hat{f}_x - f_x)^T (\hat{f}_x - f_x). \tag{22}$$

Eq. (22) shows that $\dot{V} \leq 0$ and V will decrease when the force estimation error $\tilde{f}_x = \hat{f}_x - f_x$ exists. Therefore, the updating law in Eq. (16) will eventually lead to $\tilde{f}_x \to 0$ when $t \to \infty$.

C. Reference Trajectory Generation

In this subsection, with the estimation of the unknown movement of DFR and the object deformation, inspired by [28], we develop an algorithm to generate a reference trajectory for AFR, such that the holding force of the held object can be sustained around a fixed value when being moved.

As shown in Fig. 2, according to Eq. (6), we set a desired force

$$f_{x,d} = k_o(x_c - x_{1,d}), \tag{23}$$

which corresponds to a desired trajectory

$$x_{1,d} = x_c - \frac{1}{k_o} f_{x,d}, \tag{24}$$

with $f_{x,d}$ representing the desired holding force and $x_{1,d}$ denoting the desired trajectory for AFR. Based on Section III-B, if we have the estimation of x_c and k_o, we can obtain the desired trajectory for AFR via Eq. (24), which will be used for comparison in Section IV to the forthcoming-developed impedance-model-based approach.

We define a target impedance model for AFR,

$$m\ddot{x}_1 + b\dot{x}_1 + k(x_1 - x_{1,d}) = e_f, \tag{25}$$

where

$$e_f = f_x - f_{x,d} \tag{26}$$

is the force tracking error, with $f_{x,d}$ as the desired force, m, b and k are positive and represent impedance parameters.

According to Eq. (6), we can write,

$$\begin{aligned} x_1 &= -\frac{1}{k_o} f_x + x_c \\ &= -\frac{1}{k_o}(f_{x,d} + e_f) + x_c. \end{aligned} \tag{27}$$

Substituting Eq. (27) into impedance model (25), we obtain

$$\begin{aligned} &m\ddot{e}_f + b\dot{e}_f + (k + k_o)e_f = \\ &-(m\ddot{f}_{x,d} + b\dot{f}_{x,d} + kf_{x,d}) + k_o(m\ddot{x}_c + b\dot{x}_c + kx_c) - kk_o x_{1,d}. \end{aligned} \tag{28}$$

As $f_{x,d}$ is constant, we have

$$\begin{aligned} &m\ddot{e}_f + b\dot{e}_f + (k + k_o)e_f = \\ &-kf_{x,d} + k_o(m\ddot{x}_c + b\dot{x}_c + kx_c) - kk_o x_{1,d}. \end{aligned} \tag{29}$$

For such force tracking error dynamics, the steady-state error is

$$e_{f,ss} = \frac{k_o}{k + k_o}(-\frac{k}{k_o} f_{x,d} + (m\ddot{x}_c + b\dot{x}_c + kx_c) - kx_{1,d}). \tag{30}$$

Consequently, to eliminate the steady-state error, we need the desired AFR trajectory to satisfy

$$x_{1,d} = \frac{1}{k}(m\ddot{x}_c + b\dot{x}_c + kx_c - \frac{k}{k_o} f_{x,d}). \tag{31}$$

Replacing x_c and k_o in Eq. (31) with the updating $\hat{x}_c$ and $\hat{k}_o$ from Eq. (23), we will have AFR's reference trajectory

$$x_{1,r} = \frac{1}{k}(m\ddot{\hat{x}}_c + b\dot{\hat{x}}_c + k\hat{x}_c - \frac{k}{\hat{k}_o} f_{x,d}). \tag{32}$$

As similarly proved in [28], we eventually have $f_x \to f_{x,d}$ as $x_{1,r}$ eliminates $e_{f,ss}$.

To summarise, we have $\hat{f}_x \to f_x \to f_{x,d} \to ||F_d||$ because i) $\hat{f}_x \to f_x$ as described in the previous subsection, ii) $f_x \to ||F||$ as f_y and $f_z \to 0$ and iii) $f_{x,d}$ is set as $||F_d||$ (e.g., $F_d = [f_{x,d}, 0, 0]^T$ in this development). This means that based on the holding line regulation, the movement-estimation-based and impedance-model-based reference trajectory $x_{1,r}$ leads to the object's contact force converging to the desired value.

IV. Simulations and Experimental Study

In this section, we conduct three groups of simulations and two experiments. Corresponding analysis of their results is given.

Since adaptation of AFR's reference trajectory requires a certain time to stabilize, we smooth it via $x'_{1,r} = x_{1,r}(1 - e^{-\mu t^\eta})$. In this way, $x'_{1,r}$ will start from zero and will be gradually dominated by $x_{1,r}$ as time goes by. $\mu = 5$ and $\eta = 1$ in all simulations and $\mu = 0.01$ and $\eta = 2$ in all experiments.

A. Simulations

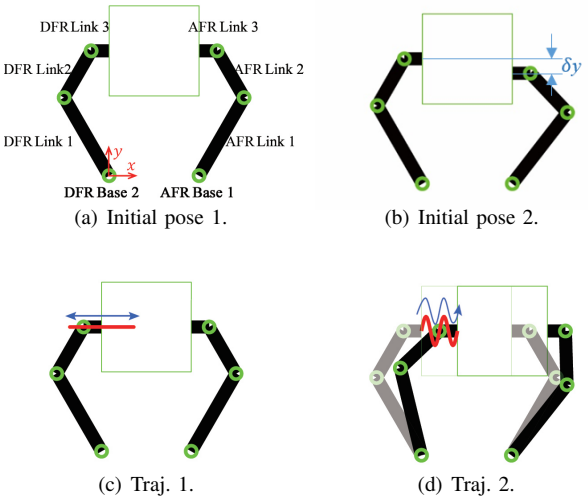

(a) Initial pose 1. (b) Initial pose 2.

(c) Traj. 1. (d) Traj. 2.

Fig. 4. The simulation platform with two 3-DOFs robots and simulation settings. (a) and (b) are two initial poses of the two robots, alternatively used in the simulations. In (c) and (d), the red lines represent DFR's trajectories and the blue lines with arrows indicating the moving directions of the trajectories.

Three groups of simulations are conducted on two 3-DOFs robots in MATLAB, as shown in Fig. 4(a), whose task space is on a two-dimensional plane. The two robots' dynamic and kinematic parameters are presented as follows. Robot links' lengths are l_{i1}, l_{i2}, l_{i3}=0.5, 0.3, 0.1 (m). Their masses are m_{i1}, m_{i2}, m_{i3}=1.5, 0.9, 0.2 (kg). AFR base coordinate is [0.5, 0] (m). DFR base coordinate is [0, 0] (m). There are two initial positions of AFR, which are shown in Fig. 4(a): $[1/3\pi, 1/3\pi, 1/3\pi]^T$(rad) and in Fig. 4(b): $[0.9112, 1.4184, 0.8120]^T$(rad), and they will be utilized alternatively for comparison purposes. DFR initial joint position is $[2/3\pi, -1/3\pi, -1/3\pi]^T$(rad). PD controller gains are Kp=diag[700, 600, 500], Kd=diag[10, 1, 0.1]. Sampling time is 10^{-3} (s) and scaling factor $s = 1$. Holding line direction is parallel to x-axis.

Two trajectories for X_l ($X_{2,d}$) illustrated in Fig. 4(c) and Fig. 4(d) are set to mimic the operator's movement. Traj. 1: $\{(x_l, y_l)|x_l = \alpha \sin \frac{2\pi}{\sigma} t, y_l = 0\}$. Traj. 2: $\{(x_l, y_l)|x_l = \beta t, y_l = \alpha \sin \frac{2\pi}{\sigma} t\}$. They are also designed for comparison purposes and will be implemented alternatively in the forthcoming simulations, where α, β and σ will be adjusted as needed.

1) Holding Line Regulation: In this group of simulations, we consider the following two cases:

Case 1: Due to calibration error or measurement noise, AFR and DFR may start a task from two different holding lines. In this part, we simulate such a case by commanding the two robots to hold and move an object with DFR teleoperated by Traj. 1 and two robots' initial positions in Fig. 4(b). To address the effect of the misalignment, Eq. (8) is applied with $k_y = 0.001$. In this case, we set $k_o = 45$, $f_{x,d} = 1$N, and in Traj. 1, $\alpha = 0.18$ and $\sigma = 20$. x_2 and k_o are assumed to be known to AFR.

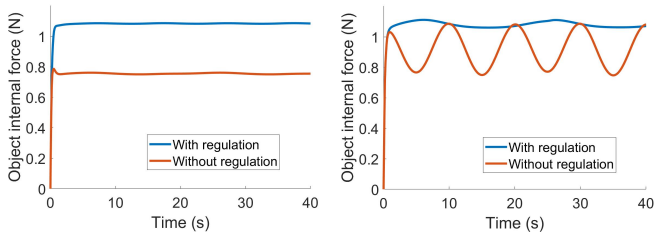

(a) (b)

Fig. 5. The holding forces in Case 1 and Case 2 in Section IV-A1.

The holding force $||F||$ is presented in Fig. 5(a). In this case, when Eq. (8) is not applied, $||D||$ is larger due to the discrepancy between two robots' actual moving directions, compared to the situation where Eq. (8) is utilized. As a result, $x_{1,r}$ also gets larger, leading to a larger distance between two EEs, which contributes to a larger error in force tracking.

Case 2: Even if both EEs are perfectly aligned in a holding line, when there is environmental disturbance acting on DFR, DFR's movement will deviate from its desired direction, which results in δy between the two EEs. In this part, we mimic such a case by using Traj. 2 and Fig. 4(a), where $\beta = 1/200$ and other settings are the same as in Case 1. Results are illustrated in Fig. 5(b).

From the above two cases, we can find how the regulation in Eq. (8) enables AFR to move up and down such that the holding line is maintained efficiently. In addition, its significance is evident in the case when DFR's deviation is relatively large. Such a case may cause failure in the task of holding and moving an object due to the insufficiently large holding force.

2) Estimation of Unknown Movement: In this group of simulations, using the proposed estimation approach in Section III-B, we will demonstrate that the desired contact force can be achieved even if we set parameters k_o and x_1 to different values. Two cases are involved, where x_c is unknown to AFR and initial values of the variables are: $\hat{k}_o = 30$(N/m) (unit "N/m" are the same for all stiffness variables in this paper and will be left out in the following), $\dot{\hat{k}}_o = 0$, $\hat{a}_0 = 0.55$, $\dot{\hat{a}}_0 = 0$, $\hat{a}_1 = 0$, $\dot{\hat{a}}_1 = 0$, $\hat{a}_2 = 0$, $\dot{\hat{a}}_2 = 0$, $m = 0.01$, $b = 0.1$ and $k = 10$. The initial position in Fig. 4(a) and Traj. 1 are employed.

Case 1: In this case, we set k_o = 25, 35 and 45 respectively, $\alpha = 0.18$ and $\sigma = 20$. Other parameters are the same as those in Section IV-A1 Case 1.

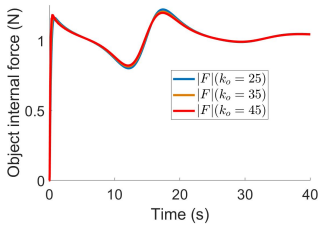

Fig. 6. Results of Case 1 in Section IV-A2.

As shown in Fig. IV-A2, f_x converges to $f_{x,d}$ in all three

conditions.

Case 2: As the movement X_2 of DFR, is unknown to AFR, we will demonstrate that when the desired force is set close to 0, the proposed adaptive estimation method can make $\hat{x}_c$ converge to x_c despite different x_2. Various x_2 are set by defining different σ in Traj. 1: σ=10, 30 and 40. k_o is set to 35 in this case and other parameters are the same as those in Section IV-A1 Case 1. Simulation results are illustrated in Fig. 7.

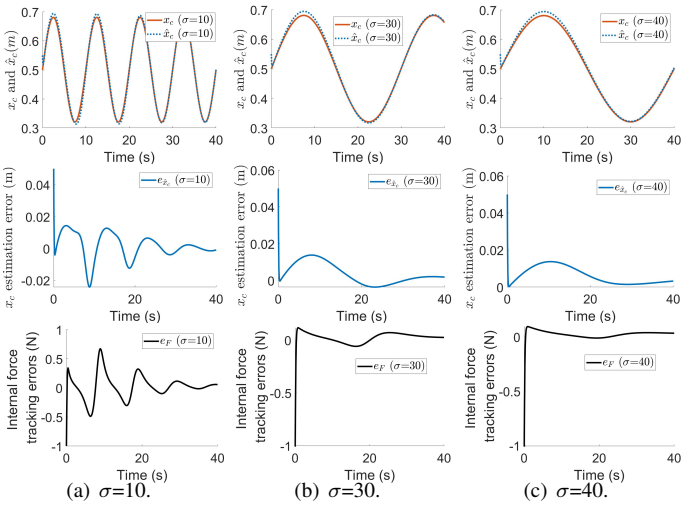

(a) σ=10. (b) σ=30. (c) σ=40.

Fig. 7. Results of Case 2 in Section IV-A2.

As shown in Fig. 7, when DFR's movement x_2 changes with σ varying from 10 to 40, $\hat{x}_c$ eventually converges to x_c (the first row) with estimation errors converging to 0 (the middle row), although the convergence takes a longer time when x_2 changes fast ($\sigma = 10$). Such an estimation makes the object's holding force converge to $f_{x,d}$ ($||F_d||$), as its tracking errors fall into a small range around 0, depicted in the third row of Fig. 7.

3) Comparison with Other Methods: To exhibit the superiority of our proposed method in detail, we design the following comparative simulations, where the proposed method in Eq. (32) is compared to the conventional force controller, the passive impedance controller [27] and the method described in Eq. (24). The force controller is described as $x_1 = 0.02(f_x - f_{x,d})$. The passive impedance controller is designed based on $e_f = m_{pi}\ddot{x}_1 + b_{pi}\dot{x}_1$ and is solved via the second order Runge-Kutta method, where $m_{pi} = 3$ and $b_{pi} = 2$.

In this comparison, we take both Traj. 1 & 2 and the robots' initial position of Fig. 4(b) into consideration, simulating a situation close to reality. $k_o = 35$ and other parameters are the same as those in Section IV-A2. Eighteen simulations under different configurations are displayed in Table I, where "F" represents the conventional force controller, "PIm" stands for passive impedance model based controller, "NoIm" is the non-impedance-based controller (Eq. (24)) and "Im" denotes our proposed impedance based controller (Eq. (32)).

We evaluate these methods by comparing the holding force tracking errors. As shown in Fig. 8, we deliberately divide eighteen simulations into three groups according to differences

TABLE I
18 SIMULATION CONFIGURATIONS.

No.	s1	s2	s3	s4	s5	s6	s7	s8
Controller	F	F	PIm	PIm	NoIm	NoIm	Im	Im
Traj. No.	1	1	1	1	1	1	1	1
Holding line regulation	No	Yes	No	Yes	No	Yes	No	Yes
f_d (N)	1	1	1	1	1	1	1	1
No.	s9	s10	s11	s12	s13	s14		
Controller	PIm	PIm	NoIm	NoIm	Im	Im		
Traj. No.	2	2	2	2	2	2		
Holding line regulation	No	Yes	No	Yes	No	Yes		
f_d (N)	1	1	1	1	1	1		
No.	s15	s16	s17	s18				
Controller	NoIm	NoIm	Im	Im				
Traj. No.	2	2	2	2				
Holding line regulation	No	Yes	No	Yes				
f_d (N)	7	7	7	7				

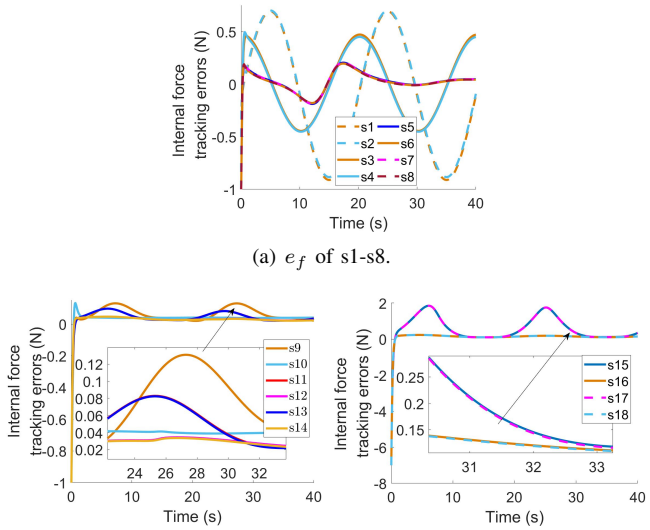

(a) e_f of s1-s8.

(b) e_f of s9-s14. (c) e_f of s15-s18.

Fig. 8. Holding force tracking results of s1 to s18.

between their tracking trajectories and f_d. Group 1 is in the light grey table. They track Traj. 1 and $f_d = 1$ and the corresponding results are depicted in Fig. 8(a). Group 2 is in the medium grey table. They track Traj. 2 and $f_d = 1$ and the corresponding results are depicted in Fig. 8(b). Group 3 is in the dark grey table. They track Traj. 2 and $f_d = 7$ and the corresponding results are depicted in Fig. 8(c). Fig. 8(a) demonstrates that the force controller achieves the worst performance, so it is not considered in the rest of the simulations. Comparing PIm to NoIm and Im in Fig. 8(a) and Fig. 8(c), it is obvious that NoIm and Im have better performance than PI. Comparing results of s3 to s4, s5 to s6, ..., and s17 to s18, where the difference between them is whether Eq. (8) is applied or not, we can conclude that Eq. (8) plays a significant role in improving the regulation of the holding line and further maintaining the holding force. From Fig. 8(b) and Fig. 8(c), we can tell that as the desired force becomes larger, the superiority of Eq. (8) becomes more evident. Similarly, comparing s5 and s6 to s7 and s8, s11 and s12 to s13 and s14, s15 and s16 to s17 and s18, we find that they all perform well because they all implement the movement estimation. Moreover, we can conclude that Im performs better than NoIm because, except for the movement estimation, Eq. (32) takes $\dot{\hat{x}}_c$ and $\hat{\hat{x}}_c$ as parts of the control input, which has the ability to predict the

movement of x and adjust $x_{1,r}$.

B. Experiments

In this section, we design a task for the SLDF teleoperation system to hold and move an object on a physical robot platform. The experiment setup is shown in Fig. 9(a), where the TouchX device is regarded as the single leader device and is manipulated by the operator, two arms of Baxter robot are treated as the dual tele-robots, a force sensor (ATI MINI45 F/T) is mounted on the left arm EE and a balloon is considered as the object to be held and moved. Baxter's right arm is directly teleoperated by the TouchX and the movement of the left arm is independently controlled based on the contact force but without using any information of the right arm. To demonstrate the holding line regulating ability, the initial poses of two EEs are set with discrepancies in x and z directions, while y axis direction is chosen as the holding line, as shown in Fig. 9(b). We set $s = 1.2$, $R = [0, -1, 0; 1, 0, 0; 0, 0, 1]$ and $n = 2$. We conduct the following two experiments to demonstrate how the proposed method works.

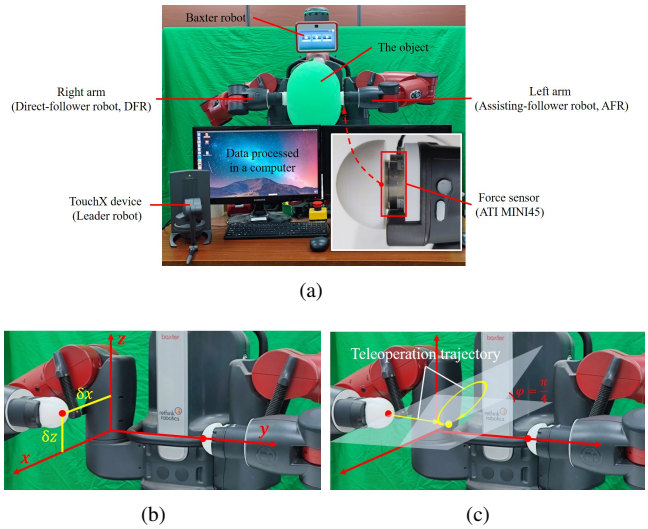

Fig. 9. The experimental setup. (a) The two arms of Baxter robot are viewed as two ***independent*** follower robots, i.e., AFR's motion regulation is generated ***not*** based on any information of DFR. (b) Discrepancies δx and δz while y direction is chosen as the holding line direction. (c) The designed teleoperation trajectory that contains movements in three directions.

1) Holding Regulation in Static Situation: We keep DFR static, while AFR is controlled to approach the object along y axis. When AFR establishes its contact with the object with a force above 1N, the proposed method is triggered in order to eliminate the discrepancies in x and z directions between two robots' EEs and to maintain the desired holding force. We set two discrepancies: $[\Delta x, \Delta z] = [0.08, 0.08]$m and $[0.1, 0.1]$m. Parameters are: $k_x = k_z = 0.0002$, initial value $\hat{k}_o = 10$, $\hat{a}_0 = 0$, $f_{y,d} = 10$N and others are the same as those in Section IV-A2. The experimental results are shown in Fig. 10.

From Fig. 10(a), we can tell that AFR adjusts its position to hold the object properly with the proposed holding line regulating method, no matter where its initial position is. From

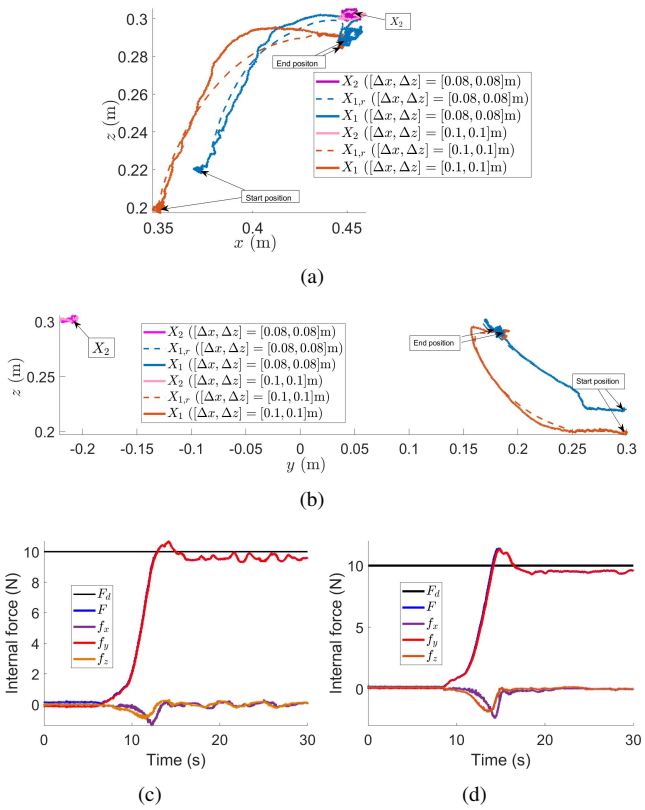

Fig. 10. (a) EE trajectories projection in xoz-plane. (b) EE trajectories projection in yoz-plane. (c) Forces with initial discrepancy $[\Delta x, \Delta z] = [0.1, 0.1]$m. (d) Forces with initial discrepancy $[\Delta x, \Delta z] = [0.08, 0.08]$m.

Fig. 10(b), we see AFR moves forward and when it contacts the object (where $y \approx 0.25$m), the movement-estimation algorithm is triggered to adjust AFR and finally move it to the same destination as they are required to make the holding forces converge to the same F_d depicted in Figs. 10(c) and 10(d). Fig. 10(c) and Fig. 10(d) also demonstrate that f_x and f_z converge to zero and f_y converges to $f_{y,d}$.

2) Continuous Movement: DFR is teleoperated along a designed trajectory shown in Fig. 9(c), which stands for a general teleoperation task that has combinations of movements in x, y and z directions, including a straight line and a curve. The initial discrepancy is set to $[\Delta x, \Delta z] = [0.08, 0.08]$m and the other parameters are the same as those in the previous experiment. For comparison purposes, the force controller and the passive impedance controller described in the simulations are also tested. The experimental results are shown in Fig. 11.

From Fig. 11(a) and 11(b), we can see that after AFR adjusts its reference trajectory to stay on the holding line, the two EEs have an approximately fixed distance, which leads to the object's holding force F staying around the desired value. From Fig. 11(c), we can find that the proposed method has better performance compared with the conventional force controller and the passive impedance controller in terms of force tracking. This is more obvious after about 20s, corresponding to the circle in Fig. 9(c) which includes forward and backward movements. A similar result can be seen in Fig. 8(a), where if DFR moves forwards and backwards in the holding line

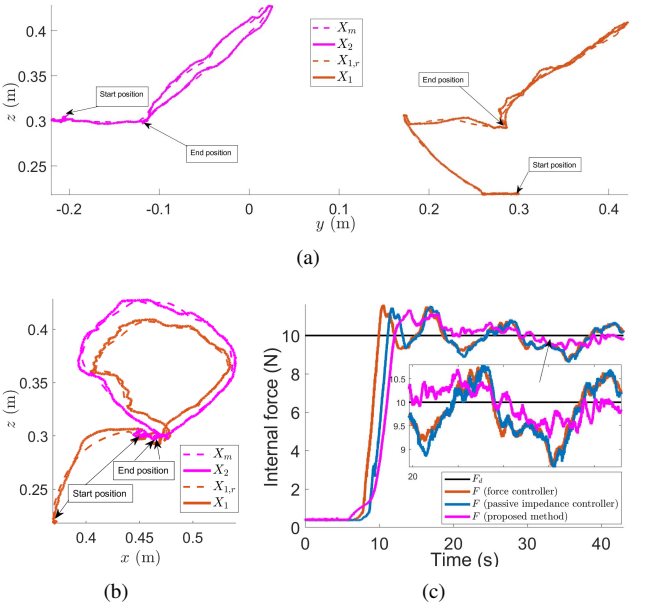

Fig. 11. (a) EE trajectories projection in yoz-plane. (b) EE trajectories projection in xoz-plane. (c) Object's holding forces under three methods.

direction, the advantage of the proposed method in regulating the holding force becomes more evident. Therefore, we can conclude that i) the proposed method is effective in regulating the holding line and maintaining the contact force; and ii) the movement estimation in the proposed method is of importance to deal with time-varying movements.

V. Conclusion

This paper introduces a method for an SLDF teleoperation system to hold and move an object, with the object's holding force maintained around a desired value. Three necessary steps are included. Firstly, the holding line regulation method is to make the robots' holding force orientation stay the same. Secondly, an adaptive movement estimation approach is used to enable the assisting tele-robot to infer its partner's movement. Thirdly, an impedance controller is derived such that the desired contact force is achieved. Comparative simulations and experiments are designed and their results verify the feasibility and effectiveness of the proposed method.

In this work, the constraint to X_c is technically addressed, but not theoretically. In the future, we will transform constraint variables such as X_c in this paper into continuous variables via, e.g., barrier Lyapunov function, making the development of the proposed method more theoretically rigorous. In addition, we will investigate more general movements that include the object's rotation. In addition, the EEs' x-/z-direction forces are still non-zero because there exist errors between the desired position and the actual position. In the future, we will model this error/offset via autoregressive model and compensate for it to achieve more accurate force tracking.

References

[1] J. E. Solanes, A. Muñoz, L. Gracia, A. Martí, V. Girbés-Juan, and J. Tornero, "Teleoperation of industrial robot manipulators based on augmented reality," *The International Journal of Advanced Manufacturing Technology*, vol. 111, no. 3, pp. 1077–1097, 2020.

[2] J. Guo, C. Liu, and P. Poignet, "A scaled bilateral teleoperation system for robotic-assisted surgery with time delay," *Journal of Intelligent & Robotic Systems*, vol. 95, no. 1, pp. 165–192, 2019.

[3] A. Birk, S. Schwertfeger, and K. Pathak, "A networking framework for teleoperation in safety, security, and rescue robotics," *IEEE Wireless Communications*, vol. 16, DOI 10.1109/MWC.2009.4804363, no. 1, pp. 6–13, 2009.

[4] W.-K. Yoon, T. Goshozono, H. Kawabe, M. Kinami, Y. Tsumaki, M. Uchiyama, M. Oda, and T. Doi, "Model-based space robot teleoperation of ets-vii manipulator," *IEEE Transactions on Robotics and Automation*, vol. 20, no. 3, pp. 602–612, 2004.

[5] H. Chen, P. Huang, and Z. Liu, "Mode switching-based symmetric predictive control mechanism for networked teleoperation space robot system," *IEEE/ASME Transactions on Mechatronics*, vol. 24, no. 6, pp. 2706–2717, 2019.

[6] R. Saltaren, R. Aracil, C. Alvarez, E. Yime, and J. M. Sabater, "Exploring deep sea by teleoperated robot-an underwater parallel robot with high navigation capabilities," *IEEE robotics & automation magazine*, vol. 14, no. 3, pp. 65–75, 2007.

[7] D.-S. Kwon, J.-H. Ryu, P.-M. Lee, and S.-W. Hong, "Design of a teleoperation controller for an underwater manipulator," in *Proceedings 2000 ICRA. Millennium Conference. IEEE International Conference on Robotics and Automation. Symposia Proceedings (Cat. No. 00CH37065)*, vol. 4, pp. 3114–3119. IEEE, 2000.

[8] R. Codd-Downey and M. Jenkin, "Wireless teleoperation of an underwater robot using li-fi," in *2018 IEEE International conference on information and automation (ICIA)*, pp. 859–864. IEEE, 2018.

[9] M. Minelli, F. Ferraguti, N. Piccinelli, R. Muradore, and C. Secchi, "An energy-shared two-layer approach for multi-master-multi-slave bilateral teleoperation systems," in *2019 International Conference on Robotics and Automation (ICRA)*, pp. 423–429. IEEE, 2019.

[10] Z. Li and C.-Y. Su, "Neural-adaptive control of single-master–multiple-slaves teleoperation for coordinated multiple mobile manipulators with time-varying communication delays and input uncertainties," *IEEE transactions on neural networks and learning systems*, vol. 24, no. 9, pp. 1400–1413, 2013.

[11] D. Sun, Q. Liao, and A. Loutfi, "Single master bimanual teleoperation system with efficient regulation," *IEEE Transactions on Robotics*, vol. 36, no. 4, pp. 1022–1037, 2020.

[12] D. Huang, C. Yang, Z. Ju, and S.-L. Dai, "Disturbance observer enhanced variable gain controller for robot teleoperation with motion capture using wearable armbands," *Autonomous Robots*, vol. 44, no. 7, pp. 1217–1231, 2020.

[13] C. Yang, X. Wang, Z. Li, Y. Li, and C.-Y. Su, "Teleoperation control based on combination of wave variable and neural networks," *IEEE Transactions on Systems, Man, and Cybernetics: Systems*, vol. 47, no. 8, pp. 2125–2136, 2016.

[14] M. Shahbazi, S. Atashzar, H. Talebi, and R. Patel, "A multi-master/single-slave teleoperation system," in *Dynamic Systems and Control Conference*, vol. 45318, pp. 107–112. American Society of Mechanical Engineers, 2012.

[15] Y. Cheung, J. H. Chung, and N. P. Coleman, "Semi-autonomous formation control of a single-master multi-slave teleoperation system," in *2009 IEEE Symposium on Computational Intelligence in Control and Automation*, pp. 117–124. IEEE, 2009.

[16] Y. Sun, B. Pan, J. Qu, and Y. Fu, "Vision-based framework of single master dual slave semi-autonomous surgical robot system," *IRBM*, vol. 42, no. 1, pp. 55–64, 2021.

[17] K. Watanabe, T. Kanno, K. Ito, and K. Kawashima, "Single-master dual-slave surgical robot with automated relay of suture needle," *IEEE Transactions on Industrial Electronics*, vol. 65, no. 8, pp. 6343–6351, 2017.

[18] B. Frank, R. Schmedding, C. Stachniss, M. Teschner, and W. Burgard, "Learning the elasticity parameters of deformable objects with a manipulation robot," in *2010 IEEE/RSJ International Conference on Intelligent Robots and Systems*, pp. 1877–1883. IEEE, 2010.

[19] J. Sanchez, J.-A. Corrales, B.-C. Bouzgarrou, and Y. Mezouar, "Robotic manipulation and sensing of deformable objects in domestic and industrial applications: a survey," *The International Journal of Robotics Research*, vol. 37, no. 7, pp. 688–716, 2018.

[20] H. Yin, A. Varava, and D. Kragic, "Modeling, learning, perception, and control methods for deformable object manipulation," *Science Robotics*, vol. 6, no. 54, 2021.

[21] W. Liang, Q. Ren, X. Chen, J. Gao, and Y. Wu, "Dexterous manoeuvre through touch in a cluttered scene," in *2021 IEEE International Conference on Robotics and Automation (ICRA)*, pp. 6308–6314. IEEE, 2021.

[22] W. Liang, Z. Feng, Y. Wu, J. Gao, Q. Ren, and T. H. Lee, "Robust force tracking impedance control of an ultrasonic motor-actuated end-effector in a soft environment," in *2020 IEEE/RSJ International Conference on Intelligent Robots and Systems (IROS)*, pp. 7716–7722. IEEE, 2020.

[23] D. Li, H. Yu, K. P. Tee, Y. Wu, S. S. Ge, and T. H. Lee, "On time-synchronized stability and control," *IEEE Transactions on Systems, Man, and Cybernetics: Systems*, 2021.

[24] Y. Hirata, Z. Wang, K. Fukaya, and K. Kosuge, "Transporting an object by a passive mobile robot with servo brakes in cooperation with a human," *Advanced Robotics*, vol. 23, no. 4, pp. 387–404, 2009.

[25] K. Iqbal and Y. F. Zheng, "Arm-manipulator coordination for load sharing using predictive control," in *Proceedings 1999 IEEE International Conference on Robotics and Automation (Cat. No. 99CH36288C)*, vol. 4, pp. 2539–2544. IEEE, 1999.

[26] R. Ikeura and H. Inooka, "Variable impedance control of a robot for cooperation with a human," in *Proceedings of 1995 IEEE International Conference on Robotics and Automation*, vol. 3, pp. 3097–3102. IEEE, 1995.

[27] F. Ficuciello, L. Villani, and B. Siciliano, "Variable impedance control of redundant manipulators for intuitive human–robot physical interaction," *IEEE Transactions on Robotics*, vol. 31, no. 4, pp. 850–863, 2015.

[28] H. Seraji and R. Colbaugh, "Force tracking in impedance control," *The International Journal of Robotics Research*, vol. 16, no. 1, pp. 97–117, 1997.

[29] S. Jung, T. C. Hsia, and R. G. Bonitz, "Force tracking impedance control of robot manipulators under unknown environment," *IEEE Transactions on Control Systems Technology*, vol. 12, no. 3, pp. 474–483, 2004.

[30] X. Zhang and M. B. Khamesee, "Adaptive force tracking control of a magnetically navigated microrobot in uncertain environment," *IEEE/ASME Transactions on Mechatronics*, vol. 22, no. 4, pp. 1644–1651, 2017.

[31] T. K. Stephens, C. Awasthi, and T. M. Kowalewski, "Adaptive impedance control with setpoint force tracking for unknown soft environment interactions," in *2019 IEEE 58th Conference on Decision and Control (CDC)*, pp. 1951–1958. IEEE, 2019.

[32] D. Ćehajić, S. Hirche *et al.*, "Estimating unknown object dynamics in human-robot manipulation tasks," in *2017 IEEE International Conference on Robotics and Automation (ICRA)*, pp. 1730–1737. IEEE, 2017.

[33] T. Wojtara, M. Uchihara, H. Murayama, S. Shimoda, S. Sakai, H. Fujimoto, and H. Kimura, "Human–robot collaboration in precise positioning of a three-dimensional object," *Automatica*, vol. 45, no. 2, pp. 333–342, 2009.

[34] S. Y. Lee, K. Y. Lee, S. H. Lee, J. W. Kim, and C. S. Han, "Human-robot cooperation control for installing heavy construction materials," *Autonomous Robots*, vol. 22, no. 3, pp. 305–319, 2007.

[35] D. J. Agravante, A. Cherubini, A. Bussy, P. Gergondet, and A. Kheddar, "Collaborative human-humanoid carrying using vision and haptic sensing," in *2014 IEEE international conference on robotics and automation (ICRA)*, pp. 607–612. IEEE, 2014.

Darong Huang is pursuing the PhD degree under the successive postgraduate and doctoral study program in South China University of Technology, China, and majors in control science and engineering. He is currently also a joint Associate Fellow in Department of Engineering and Design, University of Sussex, UK. His research interests include robot teleoperation, multiple robots collaboration, human-robot interaction and intelligent control strategies.

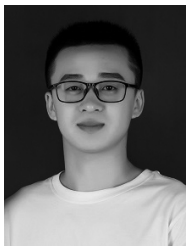

Bin Li was born in Heze, China. He received the B.S. degree from the Shandong University of Technology, Zibo, China, in 2016 and the M.S. degree from Northeast Electirc Power University, Jilin, China, in 2020. He is currently pursuing the doctor's degree with South China University of Technology, Guangzhou, China.

His research interests include manipulators, learning from demonstration and barrier Lyapunov control.

Yanan Li (M'14-SM'21) received the BEng and MEng degrees from the Harbin Institute of Technology, China, in 2006 and 2008, respectively, and the PhD degree from the National University of Singapore, in 2013. Currently he is a Senior Lecturer in Control Engineering with the Department of Engineering and Design, University of Sussex, UK. From 2015 to 2017, he has been a Research Associate with the Department of Bioengineering, Imperial College London, UK. From 2013 to 2015, he has been a Research Scientist with the Institute for Infocomm Research (I2R), Agency for Science, Technology and Research (A*STAR), Singapore. His research interests include robot control and control theory and applications.

Chenguang Yang (M'10-SM'16) received the B.Eng. degree in measurement and control from Northwestern Polytechnical University, Xi'an, China, in 2005, the Ph.D. degree in control engineering from the National University of Singapore, Singapore, in 2010, and postdoctoral training in human robotics from the Imperial College London, London, U.K. His research interest lies in robotics and automation. Dr Yang was a Recipient of the IEEE Transactions on Robotics Best Paper Award (2012) and IEEE Transactions on Neural Networks and Learning Systems Outstanding Paper Award (2022) as lead author.